Journal of Constructional Steel Research 95 (2014) 90–105

Contents lists available at ScienceDirect

Journal of Constructional Steel Research

Experimental research and cyclic behavior of buckling-restrained braced composite frame

Mingming Jia *, Dagang Lu, Lanhui Guo, Lin Sun

School of Civil Engineering, Harbin Institute of Technology, 73 Huanghe Road, Harbin 150090, PR China

ARTICLE INFO

Article history:
Received 3 May 2013
Accepted 23 November 2013
Available online xxxx

Keywords:
Buckling-restrained brace
Concrete-filled steel tube
Composite frame
Cyclic behavior
Welded splices connection

ABSTRACT

The pseudo-static tests (PSTs) of one 1/3 scale 2-story 1-bay buckling-restrained braced composite frame (BRBCF) system consisting of concrete-filled circular hollow section (CHS) steel columns, steel beams and BRBs were tested in Harbin Institute of Technology, a same bare composite frame (CF) was tested to compare with BRBCF. The test BRBCF exhibited excellent performance and sustained no strength or stiffness degradation during the significant drift demands imposed by the subsequent quasi-static cyclic test, which possessed good ductility and energy dissipation capacity. Compared with CF system, the stiffness, load-bearing capacity and energy dissipation capacity of BRBCF system increased evidently. The welded splices beam–column-BRB connections are cheap joints and are convenient to install BRBs in construction site, the experiment demonstrated their ability to withstand major ductility demands. The BRBs didn't show global buckling, local buckling and fracture of inner cores. Test also found the damage in beam–column–BRB connections region, including fractures of the gusset and beam welds, local buckling of flanges and webs of beams and enforced loops due to frame and brace action forces, which should be considered in the design of BRBCF. For frames using the proposed gusset connection, the maximum frame drift prior to failure will be governed by the rotational capacity of the beam-to-column connection, not the axial deformation of the BRB. The fracture and buckle of CHS steel tubes at the first story base indicated the thickness of CHS steel tube of composite columns in BRBCF should be enlarged to avoid the early failure of composite columns.

1. Introduction

Steel braces are used as an economic means of providing lateral stiffness to a steel structure. However, the ductility and energy dissipation capacity of a steel braced structure subjected to earthquakes are limited due to buckling of braces with unsymmetrical mechanical behavior in tension and compression. The braced frame typically exhibits substantial deterioration of strength when loaded in compression monotonically or cyclically. If the buckling of a steel brace is restrained and the same strength is ensured in both tension and compression, stable performance of braces will be assured and the ductility and hysteretic behavior will be improved [1–3]. The buckling-restrained brace consists of a steel core encased in a steel tube filled with concrete. The steel core carries the axial load while the outer tube, via the concrete (buckling–restraining mechanism), provides lateral support to the core and prevents global and local buckling. A thin layer of unbounded material along the steel core at the concrete interface eliminates shear transfer during elongation and contraction of the steel core and also accommodates its lateral expansion in compression. It is the ability of the steel core to contract and elongate freely within the confining steel concrete-tube assembly that leads to the name unbounded brace (UB). Results from past studies [2–6] showed that BRBs can undergo fully-reversed axial yield cycles without loss of stiffness or strength, which exhibits similar yielding and ultimate strength and good seismic energy dissipation, and the ultimate ductility and cumulative plastic ductility of that are quite beyond demand.

A 0.7-scale one-bay one-story Buckling-Restrained Braced Frame (BRBF) was tested under cyclic displacement histories by Aiken et al. [7] at the University of California, Berkeley. Cracks occur in the beam, column, beam–column–brace connections and gusset plates due to torsional buckling of the beam and out-of-plane displacement of the BRBs. Tsai et al. [8,9] conducted two tests on big-scale BRBFs at the National Center for Research on Earthquake Engineering (NCREE). Long brace-gusset plate connection of BRBs leaded to buckling of gussets at story drift of 0.01 rad. The cyclic behaviors of five full-scale one-bay one-story BRBFs were tested by Christopulos [10]. BRBs were connected to the frame with gusset plates and bolts; and beams were connected to the columns with single-plate shear tabs. The beams and columns close to BRB connections yielded and buckled, and then BRBs failed. Roeder et al. [11] conducted the tests of five full-scale one-bay one-story BRBFs at the University of Washington. The performances of BRBFs were influenced by gusset plate geometry, type of bolted

* Corresponding author at: Room 505, School of Civil Engineering, Harbin Institute of Technology (HIT), 73 Huanghe Road, Nangang District, Harbin 150090, China. Tel.: +86 451 86283199 505; fax: +86 451 86282704.
E-mail address: jiamingming@hit.edu.cn (M. Jia).

0143-974X/$ – see front matter © 2013 Elsevier Ltd. All rights reserved.
http://dx.doi.org/10.1016/j.jcsr.2013.11.021

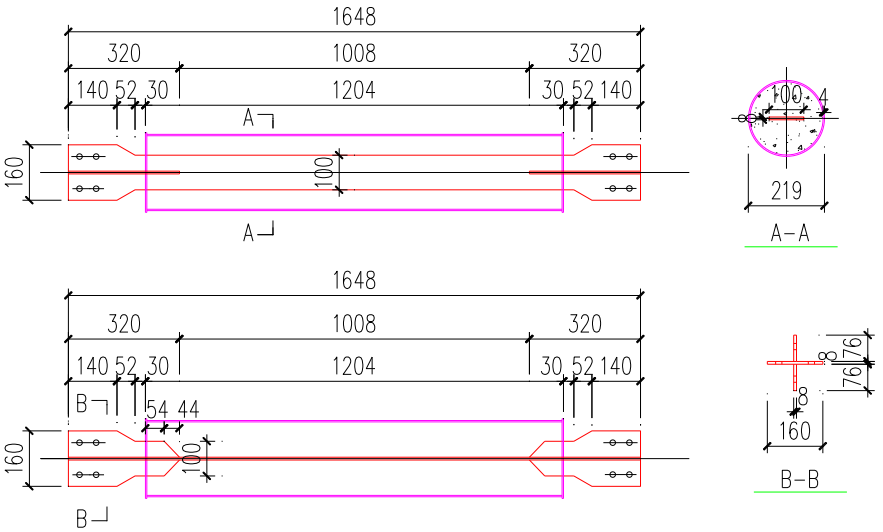

Fig. 1. Details of BRB specimens.

brace–gusset plate connection, and orientation of the BRB core plate. Failures of BRBFs were attributed to out-of-plane distortion of the BRB at story drift ratio between 0.022 and 0.024. Fahnestock and Victoria [12] did the experimental research of a 0.6-scale four-story BRBF by using hybrid pseudo-dynamic earthquake simulations and quasi-static cyclic loading. The beams were connected to beam stubs using bolted web splices and BRB were pinned to gusset at beam–column joints. During the earthquake simulations, the frame did not exhibit substantial deterioration of strength and stiffness at a story drift ratio of 0.48. The test was finished when yielding segments of inner core of BRBs fractured. It is concluded that the frame with proper design had the ability to withstand severe earthquake and maintain its load-bearing and deformation capacity. It is found that one main failure mode of BRBF is the fracture of beam–column–brace gusset welds due to frame action. A four-story BRBF tested by Victoria and Fahnestock [13] was analyzed based on a three-dimensional FE mode in ABAQUS, which was calibrated with test results. The influences on global structural response and local connection demand for different types of connection configurations are studied. BRBFs may not allow the braces to realize their full ductility capacity due to connection failure modes. Connection configuration is shown to have a significant impact on global system response and localized connection demand.

Chou and Chen [14] proposed an inelastic plate buckling equation together with coefficient charts to predict ultimate load of gusset plate connections of BRBF. Free-edge stiffeners welded to central gusset plates were demonstrated to be an effective way to increase yielding load or post-yield strength of gusset plate connections. The dual gusset plates sandwiching a BRB core reduce gusset plate size, eliminate the need for splice plates, and enhance connection stability under compression. Chou and Liou [15] conducted the experimental and nonlinear finite element analysis program to investigate ultimate compression load and bending rigidity by testing ten large dual-gusset-plate connections used for BRBFs. The ultimate compression load of the dual-gusset-plate connection was reasonably predicted by suggested computation model. A design procedure which considers both frame and brace action forces on the corner gusset connections was proposed by Chou and Liu [16]. The research of Chou and Liu [17] found that without free edge stiffeners, the single corner gusset plate buckled at a significantly lower strength and the buckling could be eliminated by using dual corner gusset plates similar in size to the single gusset plate. At low drifts, the frame action force on the corner gusset was of the same magnitude as the brace force. At high drifts, however, the frame action force significantly increased and caused weld fractures at column-to-gusset edges.

Jeffrey [18] proposed a novel connection where the gusset is only connected to the beam and is offset from the column face. A three-story frame with the novel connection was tested under quasi-static cyclic loading. The connection can withstand 3% frame drift and the

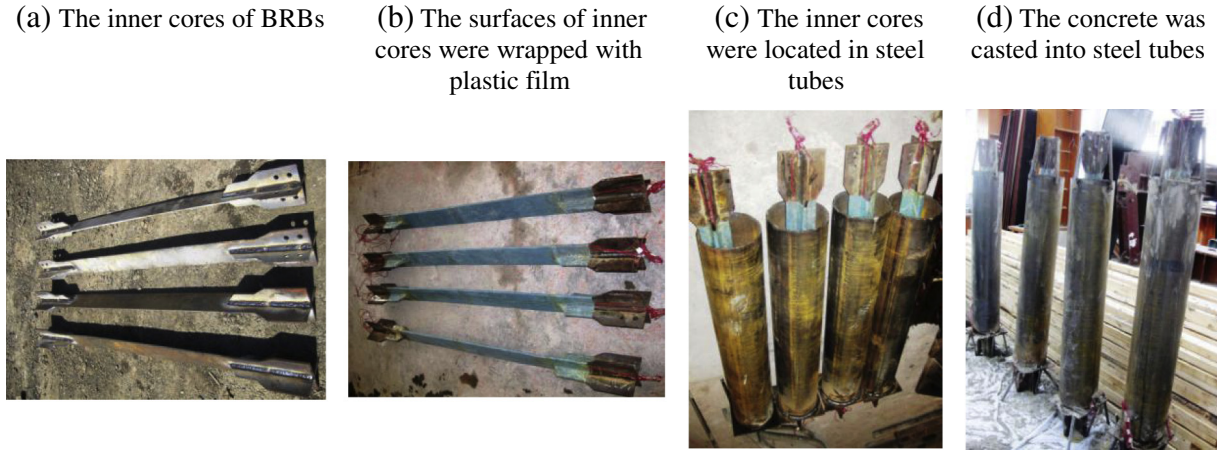

Fig. 2. Fabrication of BRB specimens. (a) The inner cores of BRBs, (b) The surfaces of inner cores were wrapped with plastic film, (c) The inner cores were located in steel tubes, (d) The concrete was casted into steel tubes.

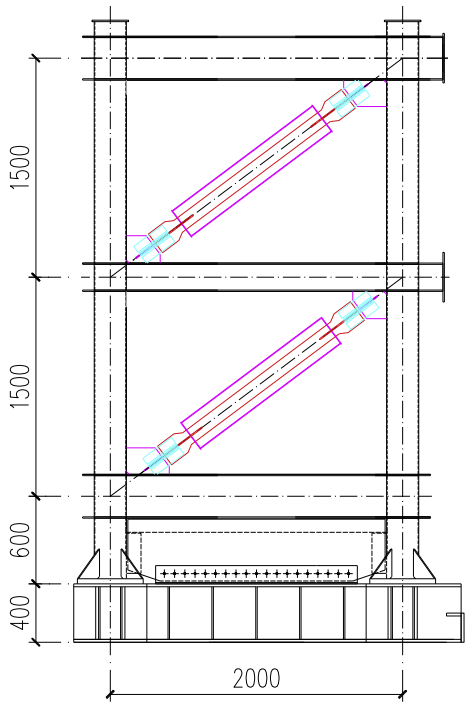

Fig. 3. Dimensions of the frame specimen.

performance of the frame is very good. Large-scale shake table tests were performed to examine the out-of-plane stability of BRBs placed in a chevron arrangement in a single-bay, single-story steel frame [19]. A simple stability model predicted the BRBs with a flexible segment at each end of the steel to fail due to out-of-plane buckling at a force smaller than the yielding strength of the steel core. It is found that BRBF provide more stable hysteretic behavior than conventional special concentrically braced frames (SCBF). A high confidence of BRBF of achieving the collapse prevention limit state was provided [20]. A three-story single-bay full-scale BRBF was tested under a series of hybrid and cyclic loading tests [21]. (BRBs) were installed in the frame specimen. BRBs include two thin BRBs and four end-slotted BRBs which all using welded end connection details. The recommendations on the seismic design of thin BRB steel casings against local bulging failure were put forward.

2. Objective and scopes

In the past, many experimental and analytical studies were done on the behavior of BRBs, but there is still limited experimental data on system-level performance of BRBFs. The studies that have been conducted on the BRBFs have also identified undesirable failure modes, such as the damage to the beam-column-BRB connections region due to frame and brace action forces, including fractures of the gusset and beam welds, local buckling on the flanges and webs of the beams and enforced loops, the fracture and buckle of CHS steel tube of composite column at the first story base. New suggestions for design improvement were proposed.

The boundary members of BRBF were almost steel columns and steel beams, and the research of BRB system with composite columns is limited. Thus, additional investigations of Buckling-Restrained Braced concrete filled steel tube column Composite Frames (BRBCFs) are needed on BRBF system on load-bearing capacity, hysteretic behavior, energy dissipation capacity, failure mode and ductility. Specially, there is rare research focused on welded splices beam–column–BRB connections, which are cheap joints and are convenient to install BRBs in construction site, so welded splices beam–column–BRB connections need to be studied.

3. Test frame and experimental setup

3.1. BRBs design and fabrication

The load-carrying element of BRB used in this paper is divided into a center yielding part and two end strengthened non-yielding parts, as shown in Fig. 1. Two end portions of inner core section are enlarged and transformed to crisscross section with welding two steel plates on both sides of original steel plate. With a smaller cross-sectional area, the center part would yield and dissipate energy via its plastic deformation. The end portions are enlarged and stiffened to supply space for connection and extra flexural rigidity for improving buckling strength. The strength of unrestrained segment in both tension and compression is larger than the ultimate strength of center part which ensures the full development of energy dissipation capacity of the center part.

The load-carrying element shortens when loaded with compressive force, whereas the length of the lateral-support element remains basically unchanged. To prevent the load-carrying element from bearing against the lateral-support element, interior reserve space should be provided at the junction between rectangle section segment and crisscross section unrestrained segment. The reservation of interior reserve space can be accomplished by inserting soft material, such as rubber, into the reserve space before casting concrete. As the load-carrying element is stressed, there is a relative movement between the load-carrying and lateral-support elements. Four layers of plastic film (0.2 mm in thickness) were applied to the surface of load-carrying element to reduce the bonding force between load-carrying and lateral-support elements [22], as shown in Fig. 2. The inner cores were located at proper place in steel tubes, one end plate was welded on one end of steel tube, and then casted concrete into steel tubes, at last another end plate was welded on the other end of steel tube. The fabrication of BRB was completed.

3.2. BRBCF design and fabrication

A two-story one-bay BRBCF was constructed as sub-assemblies of a building over two floors. The height of story was 4.5 m, and the span with BRB was 6 m. The specimen providing lateral load resistance was considered in this study, which was designed according to Chinese code for seismic design of buildings (GB50011-2010), Chinese code for design of steel-concrete composite structure (DL/T5085-1999) and Chinese code for design of steel structure (GB50017-2003). The

Table 1
Detail dimensions of buckling-restrained braced composite frame specimen.

Story height (mm)	Span (mm)	Column section $D \times T$ (mm)	Beam section of middle beam (mm)	Beam section of top and bottom beams (mm)	Steel of beam	Steel of steel tubes	Concrete in steel tubes
1500	2000	219 × 4	H194 × 150 × 6 × 9	H300 × 150 × 6.5 × 9	Q235B	Q235B	C30

Table 2
Mechanical properties of steel.

Steel	Properties					
	Yield stress f_y (N/mm^2)	Tensile strength f_u (N/mm^2)	f_u/f_y	Elastic modulus E_s ($\times 10^5$ N/mm^2)	Poisson ratio ν	Elongation ratio δ (%)
Steel tube of column	298	366	1.23	2.032	0.287	31.70
Steel of beam	261	413	1.58	2.058	0.287	26.94
Steel plate of BRB	263	379	1.44	2.030	0.287	25.00

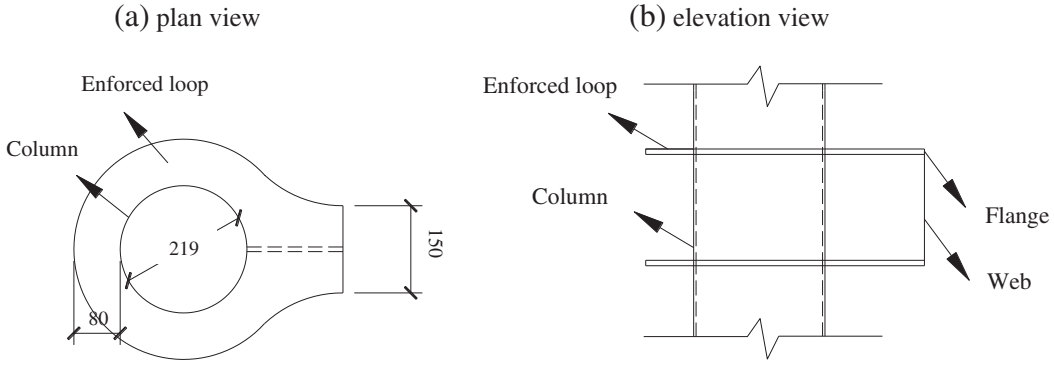

Fig. 4. The details of the moment connections. (a) plan view. (b) elevation view.

designed structure is located on firm rock (site class II in GB50011-2010). The fortification intensity and the design characteristic period of the location site are 9° and 0.35 s, respectively. The total seismic building weight is 100 kN, the seismic design base shears for minor earthquake and major earthquake are 32 kN and 140 kN, the seismic design base shear of structure is specified as $V_{des} = 140$ kN.

According to the loading capacity of actuator, one 1/3 scale specimen with one-bay, two-and-half-story was designed and fabricated. In the design, the rigidity of composite column and boundary beam should satisfy the capacity design principle considering the strain-hardening braces and an unbalanced vertical load resulted from the difference of the peak BRB compressive and tensile strengths. The story height is 1500 mm, and the span length is 2000 mm. The dimensions of the frame are given in Fig. 3. The specimen includes composite moment frame and BRBs. The frame consists of concrete-filled circular hollow section (CHS) steel tube columns and steel beams. In the design, the final selections of structural members are given in Table 1; the section of circular steel tubes is 219 × 4 (mm, diameter x thickness, $D \times T$); the H section of middle beam is 194 × 150 × 6 × 9 (mm, flange width × web height × flange thickness × web thickness); and the H section of top and bottom beams are 300 × 150 × 6.5 × 9 (mm, flange width × web height × flange thickness × web thickness). BRBs with a rectangular inner core have a section of 100 × 8 (mm, width × thickness). There is a half story at the bottom of the frame as shown in Fig. 3, the half story height is 600 mm. The aim of this construction was to install the load actuators on the reaction wall, and ensure the same height for the first story and the second story. The 6 mm thickness steel plate welded in the half story was used to strengthen this story. The steel plate was fixed on rigid base beam with a row of bolts and can be removed with the frame from the footings after one test.

To determine the steel material properties, three tensile coupons were cut out from each steel plates used for inner cores of BRBs and tested in accordance with the Chinese standard: Steel and steel products–Location and preparation of test pieces for mechanical testing (GB/T2975-1998). The actual material coupon material properties are given in Table 2. All steel is Chinese Q235B with nominal yield stress of 235 MPa, where f_y, f_u, E_s, ν, δ are steel yield stress, tensile strength, elastic modulus, Poisson ratio and elongation ratio, respectively. The test result showed that the yield stress of steel plates of inner cores of BRBs is 263 N/mm^2 and tensile strength is 379 N/mm^2 (1.44 times of its yield strength), ultimate strain of Q235B steel is 25%. The outer circle steel tubes are 219 × 4 mm (Diameter × steel tube wall thickness), yield stress $f_y = 298$ MPa, tensile strength $f_u = 366$ MPa (1.23 times of its yield strength), ultimate strain of Q235B steel is 31.7%.

Fig. 5. Beam–column connection details.

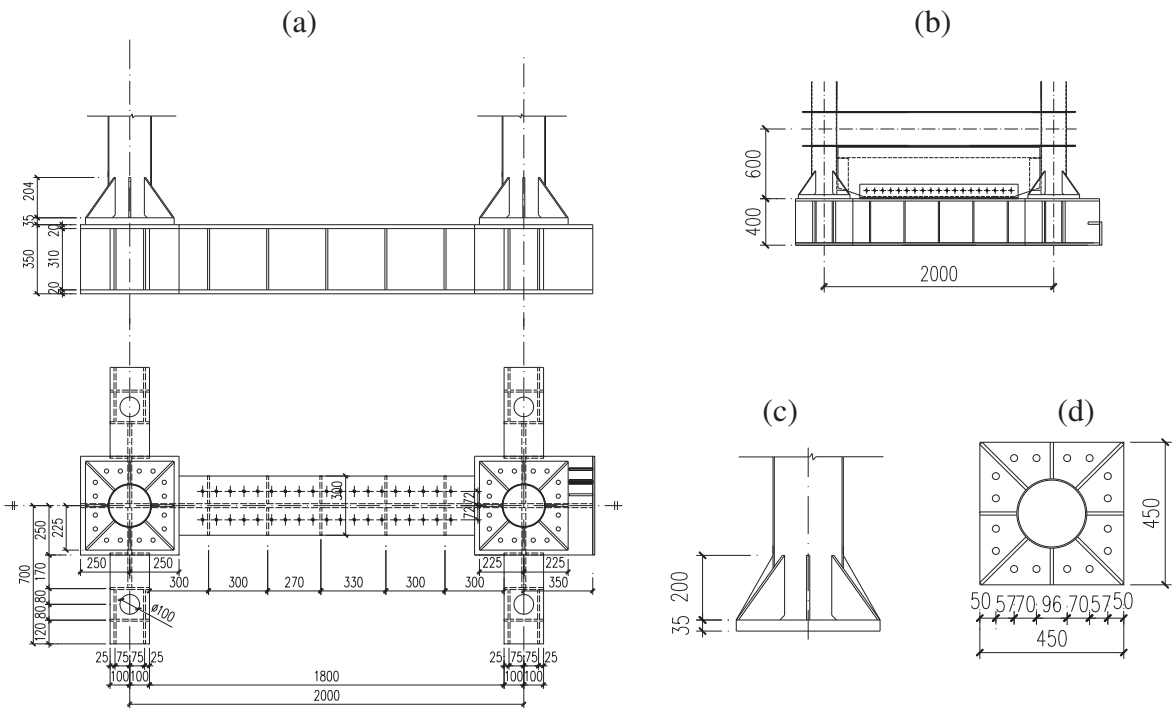

Fig. 6. The details of footing of BRBCF.

After the steel member was fabricated, the hollow steel columns were then filled with plain concrete in a vertical position. The concrete filled in steel tubes was properly vibrated to eliminate air pockets in the concrete and to produce a homogeneous mix. Three 100 mm cubes were cast for each batch of concrete mix. These were cured in similar conditions as concrete in steel tubes. The tests of these concrete cubes were carried out in accordance with the Chinese standard: Testing methods for mechanical performance of common concrete (GBJ81-1985). The average compression stress of the in-filled C30 concrete in the CHS steel columns is 28.92 MPa.

The details of the moment connections are schematically given in Fig. 4. The enforced loop was applied to connect the composite column and steel beam, the dimension of which was selected according to Chinese code for design of steel-concrete composite structures (DL/T5085-1999). The pictures of beam–column connection details are shown in Fig. 5.

In this 1/3 scale test, being subjected to the large force demand induced by axial force of columns and braces, the footings need to be strengthened by some measures. The details of the footings are shown in Fig. 6. Bolts and stiffener were employed to fix the columns on the rigid base beam and then anchor bolts were employed to fix the rigid base beam on the floor to raise the capacity of the footings. So the frame specimen was connected to rigid base beam at the bottom story through connections capable of transferring the plastic moment capacity. The rigid base beam was then fixed on the strong floor to prevent uplift of the frame specimen during testing.

One BRB was installed concentrically in one story, 8 unconstrained splice plates were used to weld each BRB end to gusset connection. Typical BRB-to-frame connection is shown in Fig. 7. Centrelines of the brace, beam, and column intersected at the center of the column panel zone and the BRB gusset is conjoint to column and beam face. As shown in Fig. 7, the work point of the gusset connection is at the intersection of the beam and column centrelines, if not, it requires additional flexural demands on the beam, but that case is not considered here.

3.3. Experimental setup

The experimental setup is illustrated in Fig. 8, the test frame is a planar structure with four in-plane attachments, namely, one load

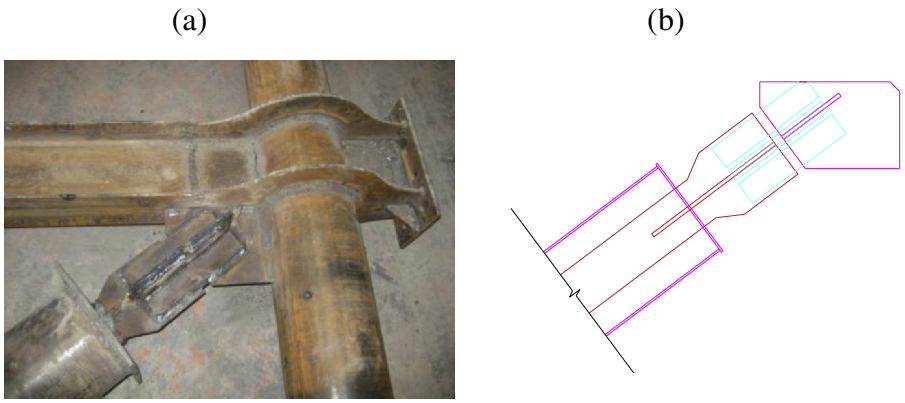

Fig. 7. The details of the BRB connections.

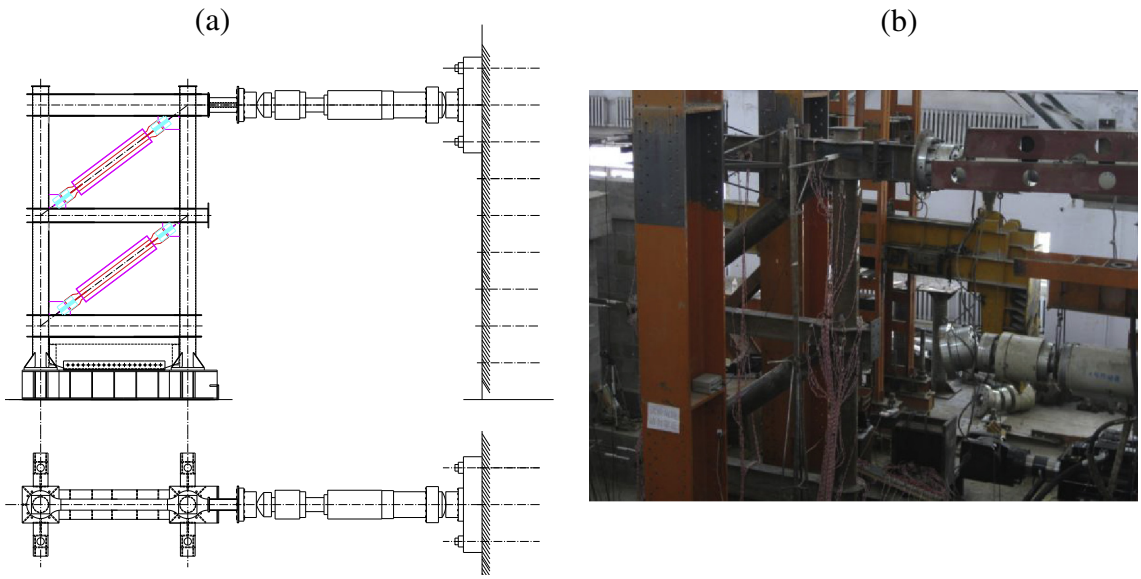

Fig. 8. The experimental setup of BRBCF.

point and three reaction points. The reaction points are two column bases that anchored to the strong floor and one ground-level links. Load was applied to the test frame at the top floor level by an actuator that was attached to the reaction wall. Instrumentations including load cells were used to measure the reactions and the applied actuator force. Loading was only applied at the top story of the frame specimen; therefore, the story shear force was equal at each level.

Out-of plane stability is provided by the dual bracing frames, the reactive frame provides negligible resistance in the plane of the frame specimen. Lateral braces are provided at the top of frame by using four rollers fixed at the quarters of top frame beam (Fig. 9).

Behavior of the boundary frame as well as BRBs during the testing was measured. Uniaxial strain gauges were placed on each column and each inner core of BRBs as shown in Figs. 10 and 11. Rosette strain gauges were placed on the steel tubes so that the principal stresses at these locations could be obtained. Linear Variable Displacement Transducers (LVDTs) were placed to measure the horizontal displacement of each story and the relative displacement between the column base and strong floor. Also, the out-of-plane deformation of the frame was measured by LVDTs. The distribution of LVDTs is presented in Fig. 12.

The load was applied in accordance with the Chinese standard: Specification of testing methods for earthquake resistant building (JGJ101-1996). In elastic range, the lateral load was applied with an increment load, incremental amplitude was one third of yielding load of structural system, and at each increment one loading cycle was applied to the frame. Once yielding was reached, the applied load was a function of the yielding displacement Δ_y. In this range, load incremental amplitude was 10 mm, three cycles of top story displacements were applied to the test frame at each displacement increment. Story displacement was assumed to be proportional to BRB deformation, story displacement is about 1.25 times of BRB deformation in this story. Top story drift was used as the control quantity here because the frame was comprised of two BRB specimens.

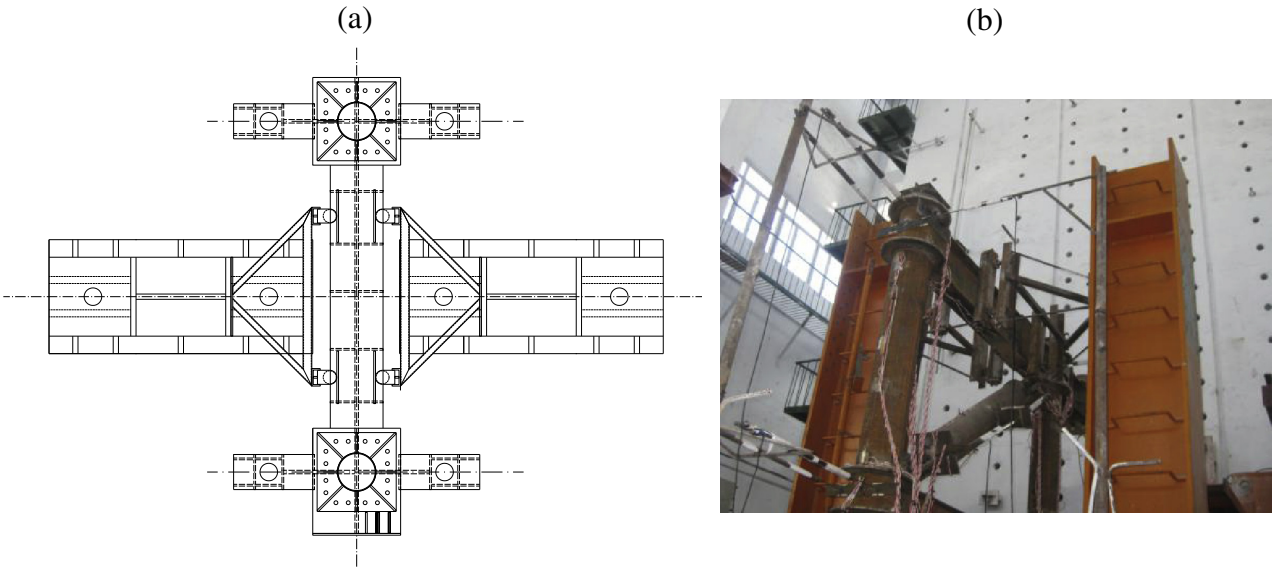

Fig. 9. Lateral braces distribution of BRBCF.

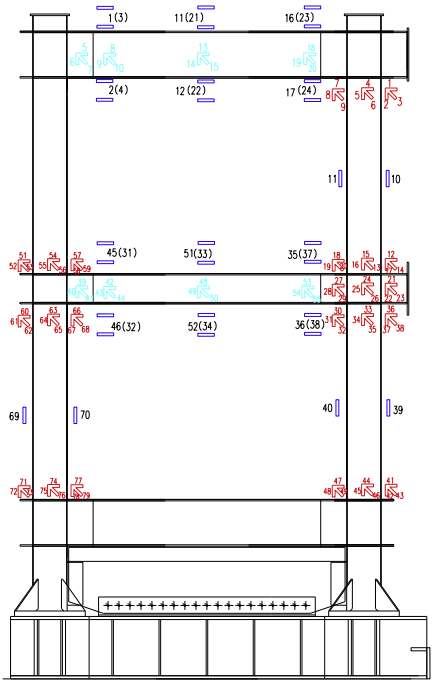

Fig. 10. Distribution of strain gauges and rosettes of CF.

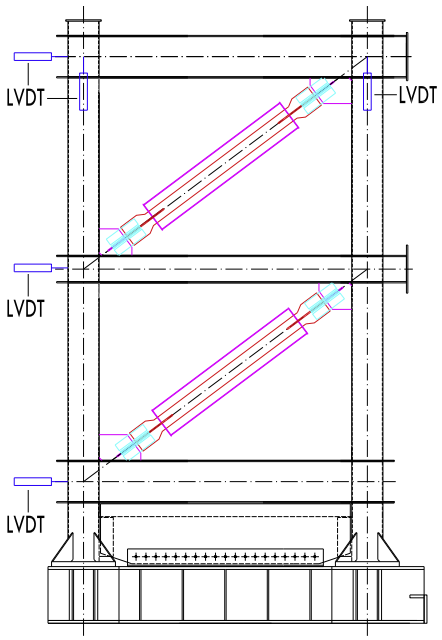

Fig. 12. Distribution of LVDTs.

4. Experimental phenomena

As shown in Fig. 13, the yielding locations of components are indicated as circle points, the numbers show the sequence of structural member yielding. In elastic range, the lateral load was applied with an increment load of 50 kN, the frame was almost elastic at the lateral load of 200 kN. Yielding was observed around bolt holes in the inner cores of BRBs at the applied actuator force of 220 kN at the top beam of the frame specimen. At the top roof drift ratio of 1/375 (drift of 8 mm), the principal strain along the yielding segments of inner cores of BRBs at the locations 1 and 2 reached its yield strain, and meanwhile the main frame remained elastic.

The stiffness of BRBCF began to decrease due to the yielding of BRBs. Note that the middle beams have the BRB connections at their faces, at the top roof drift ratio of 1/75 (drift of 40 mm), the flange of middle beam at the locations 3 and 4 yielded near the beam–column-brace connections. During the cycles of sequence at top roof drift ratio of 1/50 (drift of 60 mm), the flange of middle beam yielded at the locations 5, 6 points opposite to 3, 4 points. The gusset plates yielded at the beam–column brace connections due to welding residual stress. At the top story drift ratio of 1/75, the web of middle beam yielded near the beam–column–brace connections at the locations 7, 8 points, and then the plastic hinge were formed at both ends of middle beam. The columns exhibited flexural and shear yielding, the column

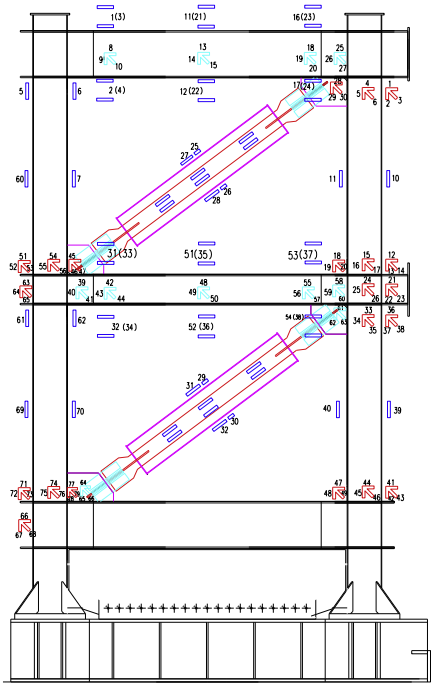

Fig. 11. Distribution of strain gauges and rosettes of BRBCF.

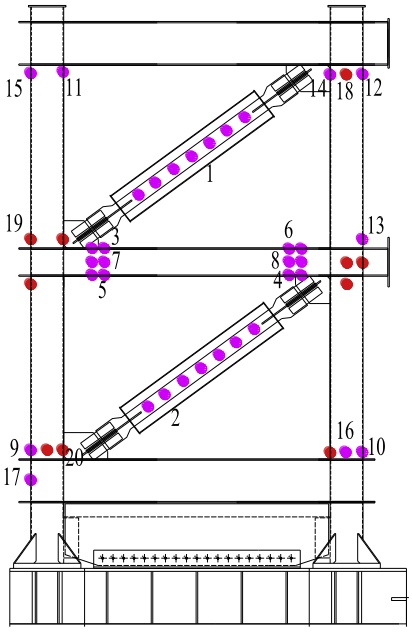

Fig. 13. Yielding locations.

(a) The bottom flange of one middle beam end buckled

(b) The buckling deformation developed to half circle

(c) A crack developedand propagated through the beam flange and into the web

(d) Out-of-plane deformationof the column

(e) Lateral braces buckled

(f) The crack of tension steel tube in the first story

Fig. 14. Experimental phenomena of BRBCF specimen. (a) The bottom flange of one middle beam end buckled. (b) The buckling deformation developed to half circle. (c) A crack developed and propagated through the beam flange and into the web. (d) Out-of-plane deformation of the column. (e) Lateral braces buckled. (f) The crack of tension steel tube in the first story.

bases began to yield at the locations 9, 10 points. During the top story drift ratio between 1/50 and 1/40, the column base, column top, beam–column connection especially the enforced loop yielded gradually. Structural members yielded at the locations 11, 12, 13 points at the top roof drift ratio of 1/50; and then yielded at the locations 14, 15, 16, 17 points at the top roof drift ratio of 2/75. At last, structural members yielded at the locations 18, 19, 20 points at the top roof drift ratio of 1/40.

The BRBs, yielded at a considerably lower drift ratio of 1/115 and were responsible for all energy dissipation prior to yielding in the frame. The results indicated that BRBs begin to yield at approximate top roof drift ratio of 1% and have significant inelastic deformation prior to the onset of frame yielding. The yielding sequence followed as BRBs, beams and columns. The main frame was protected due to the function of BRBs, excellent load-bearing capacity and ductility of BRBCF were confirmed during earthquake.

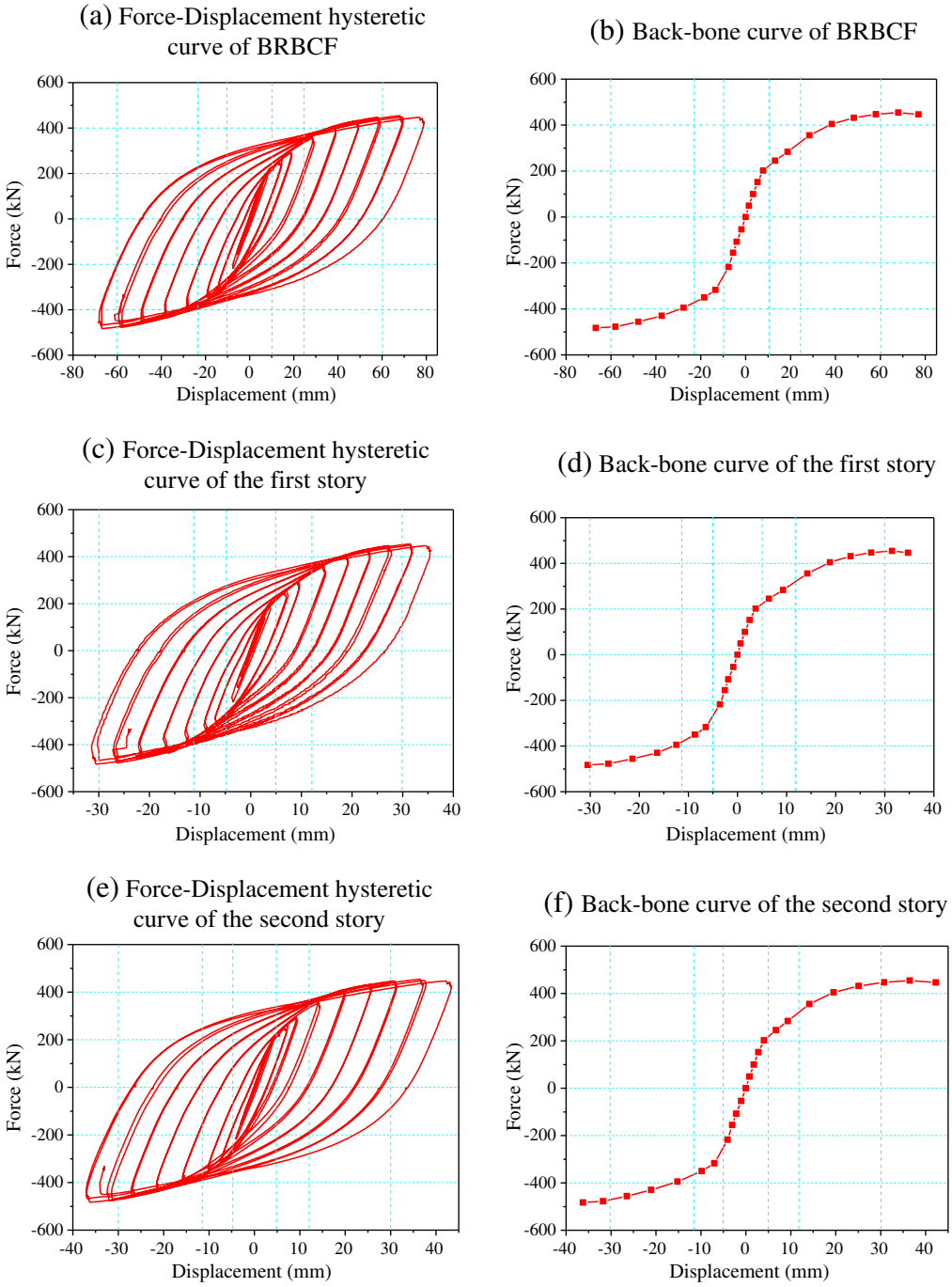

Fig. 15. Force-displacement hysteretic curves and back-bone curves. (a) Force-displacement hysteretic curve of BRBCF. (b) Back-bone curve of BRBCF. (c) Force-displacement hysteretic curve of the first story. (d) Back-bone curve of the first story. (e) Force-displacement hysteretic curve of the second story. (f) Back-bone curve of the second story.

During the cycles of sequence at approximate top roof drift ratio of 1/50, the buckling deformation developed gradually on the compression column near the base of the first story, and the steel tube of tension column near the base of the first story was torn along the horizontal direction near the beam–column–brace connection. At the top story drift ratio of 7/300, the buckling deformation on the first story compression column near the base developed severely, the bottom flange of one middle beam end buckled according to BRBs axis load (As shown in Fig. 14(a)). So stiffeners should be welded on beam web in the lines of gusset edges. A crack initiated in the first story tension column base and then developed, the welding line of steel tube under enforced loop fractured, the crack is 2 mm width and 5–6 mm length.

During the cycles of sequence at approximate top roof drift of 80 mm, loud banging noises were attributed to slip in the bolted connections of structural system. The buckling deformation on the first story compression column base developed to half circle (As shown in Fig. 14(b)), both middle beam ends buckled at the bottom flange. A crack developed in a weld which is at the middle beam end, and then propagated through the beam flange and into the web (As shown in Fig. 14(c)). Compared to the BRB, the frame exerted a larger force on the gusset at high drift levels, which caused the gusset edges to fracture. The crack was caused by frame action on the gusset plate as observed in the previous BRBF test (Chou and Liu, 2012). This fracture led to large torsional rotations of the top beam and out-of-

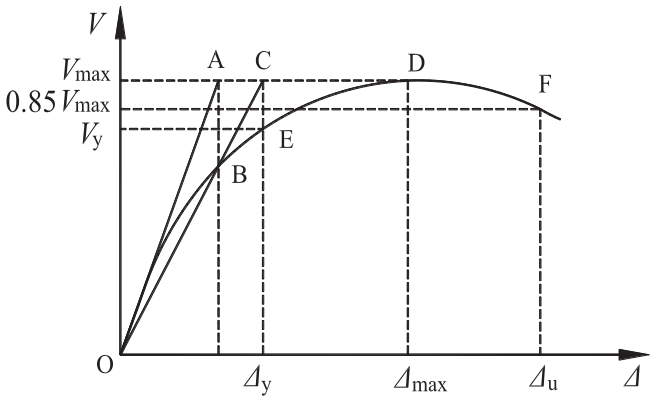

Fig. 16. Schematic diagram of graphing method.

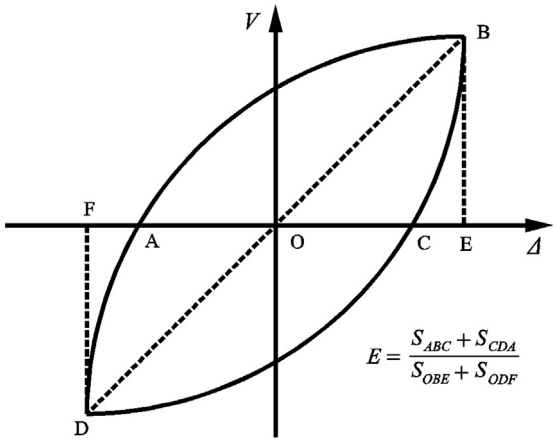

Fig. 18. Calculation of energy dissipation coefficient.

plane displacement of the column that connected to the actuator (As shown in Fig. 14(d)). It was found that the lateral braces buckled as shown in Fig. 14(e), so the test stopped at this load level. After the test, the buckling deformation on the first story compression column base developed to almost one circle, the crack in the first story tension steel tube under enforced loop developed to 4–5 mm width and 10–12 mm length (As shown in Fig. 14(f)).

Despite the large displacement imposed on the BRBs in the test, the BRBs exhibited good performance during the quasi-static cyclic test. The frame specimen behaved in a ductile manner, there was evidence of yielding, significant plastic deformation on BRBs, beams and columns, obvious local buckling and fracture of the beam flanges occurred at the joints according to frame action and BRBs axis load. There is evident buckling and cracks in the column base of the first story.

Fractures of the gusset edges were caused by the opening and closing of the angle between the column and beam at the beam-to-column connection, the frame exerted a larger force on the gusset at high drift levels due to frame action. When opening, tensile stresses oriented approximately perpendicular to the BRB's longitudinal direction developed in the gusset and must be transferred through the gusset weld to the beam and column, cracks occurred in a weld at the beam end which is close to the beam-to-column connection. When closing, the gusset plate was compressed but didn't buckle. If the gusset does buckle, the out-of-plane deformation would cause additional compression and tension stresses in the welds. Even if buckling did not occur the alternating cycles, tension and compression stresses exerted by the frame from low-cycle fatigue could initiate fracture of the gusset weld and beam weld.

5. Hysteretic curves and backbone curves

The top story drift is equal to the displacement of LVDT at top beam distracting the displacement of LVDT at middle beam, and the first story drift is equal to the displacement of LVDT at middle beam distracting the displacement of LVDT at bottom beam. The story drift ratio is equal to the story drift divided by the story height.

The base shear versus roof drift is shown in Fig. 15(a). Elastic specimen behavior was observed during the first two cycles, which is shown as a small hysteretic area in the early cycles of Fig. 15(a). The story shear force versus story drift plots in Fig. 15(c), (e) illustrate the excellent global performance of the test frame. Fig. 15(b), (d), (f) show the backbone curves of structure and two stories taken as the connecting line of peak points of each cycle of hysteretic loops. The backbone curves for the BRBCF were conducted to obtain the force-displacement relationship. Fig. 15(b) shows the relationship between base shear and roof drift of the BRBCF, Fig. 15(d), (f) show the relationships between the story shears and story drifts of the BRBCF.

As shown in Fig. 16, the yielding loads of structures are determined based on 'graphing method'. The point A is the intersection of tangent line of curve through the origin and horizontal line through the peak point D of backbone curve. The point B is the intersection of the perpendicular line from point A to Δ axis and backbone curve. The extended line of OB intersects at point C with line AD. The point E is the intersection of the perpendicular line from point C to Δ axis and backbone curve. The load corresponding to point E is yielding load V_y, the load corresponding to peak point D is maximum load, the slope of line OC is secant stiffness of structure. The displacement corresponding

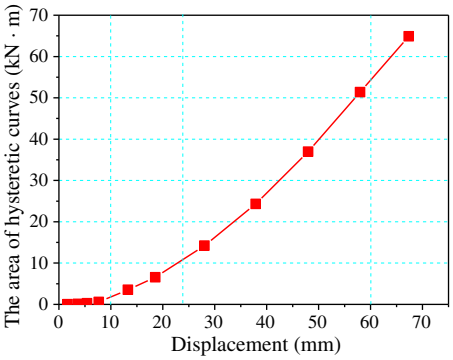

Fig. 17. The relationship curve of area of hysteretic curves versus story drift.

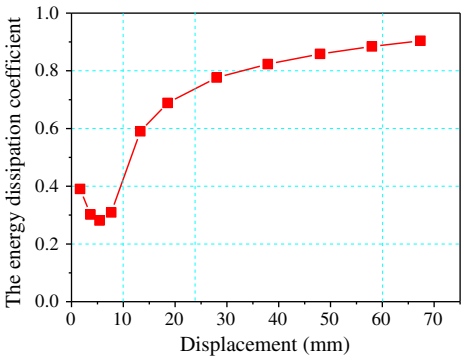

Fig. 19. The relationship curve of energy dissipation coefficient versus story drift.

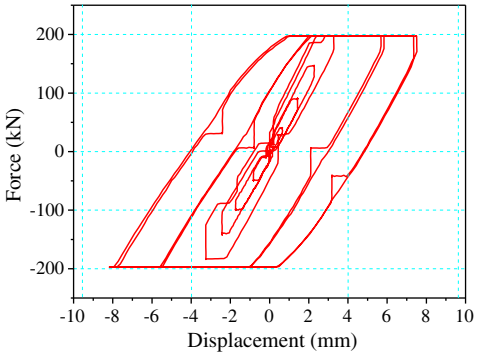

Fig. 20. The hysteretic curves of BRB measured by strain gauge.

to point E is yielding displacement Δy. The point F at backbone curve corresponds to 85% maximum load, the displacement corresponding to point F is ultimate displacement Δu. The ratio of ultimate displacement Δu and yielding displacement Δy is ductility of structure.

As shown in Fig. 15(b), positive first–yield strength, V_{y1}, of the BRBCF was 200 kN ($=1.43\ V_{des}$) when BRBs yielded at a roof drift ratio of 1/375. The base shear reached 400 kN ($=2.86\ V_{des}$) and 450 kN ($=3.21\ V_{des}$) corresponding to yielding of structural members in the beams and columns. According to 'graphing method' shown in Fig. 16, the positive yielding force of BRBCF is confirmed as 313 kN, overstrength calculated using the yield force divided by the design force of 140 kN is 2.24. The structure will remain elastic under major earthquake.

Fig. 15 shows symmetrical mechanical behavior of BRBCF in tension and compression, and BRBCF don't exhibit substantial deterioration of strength and stiffness when loaded cyclically. The ductility, hysteretic behavior and energy dissipation capacity of BRBCF are superior. As expected, BRBs had more strain hardening and developed larger strengths in compression than in tension due to confinement of the lateral strains provided by the restraining material, so the stiffness of BRBCF at negative displacement is larger than that at corresponding positive displacement. The figures in Fig. 15 also show the clear tri-linear behavior of the frame well beyond the drift levels where the BRBs and the main frame yield in proper sequence, consistent with

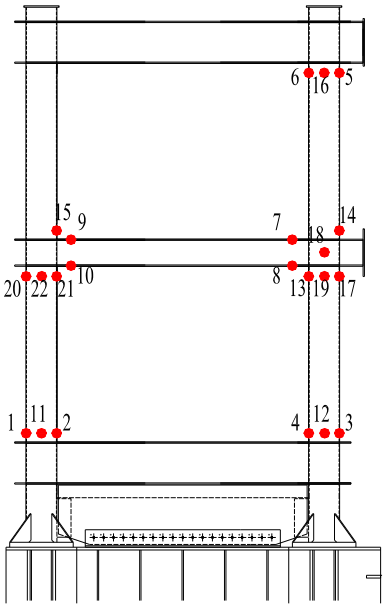

Fig. 22. Yielding locations.

the structural fuse concept. The upper story has a similar stiffness relative to the first story as indicated in Fig. 15. The portion of shear force carried by the second story is nearly same as the first story. The load–displacement hysteretic relationship curves also show that the relative deformations of the first and second story are similar; however, during the final several cycles, the second story begins to absorb more of the total frame deformation.

The positive yielding displacement is 24.51 mm and yielding force is 313 kN; the negative yielding displacement is 23.79 mm and yielding force is 376 kN. The elasto-plastic story drift ratio limit is 1/150 according to Chinese code for seismic design of buildings (GB50011-2010), so the structural drift is much less than drift limit under seismic design base shear. The positive maximum drift ratio is 1/39 and ultimate force is 454 kN; the negative maximum drift ratio is 1/44 and ultimate

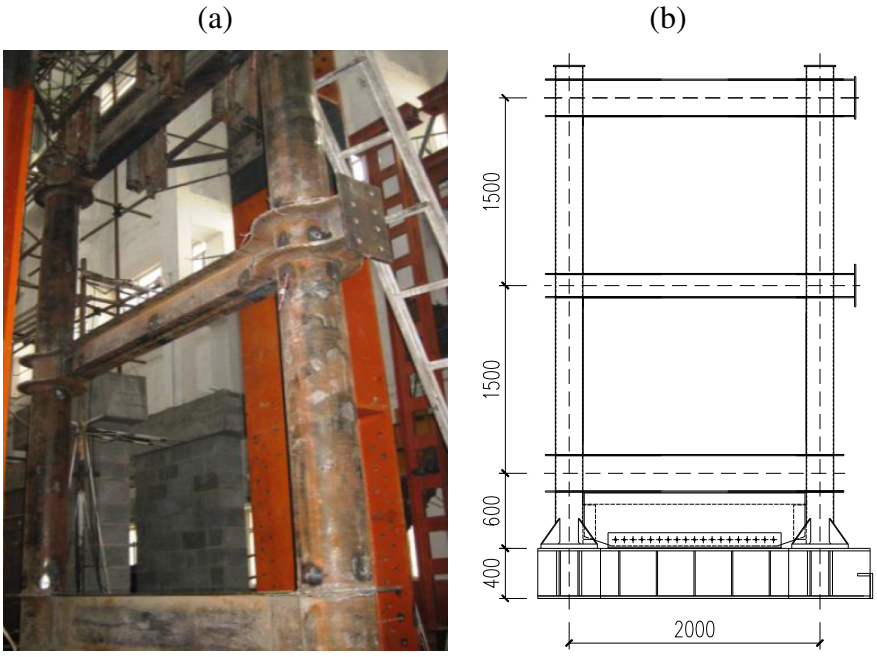

Fig. 21. CF specimen and dimensions.

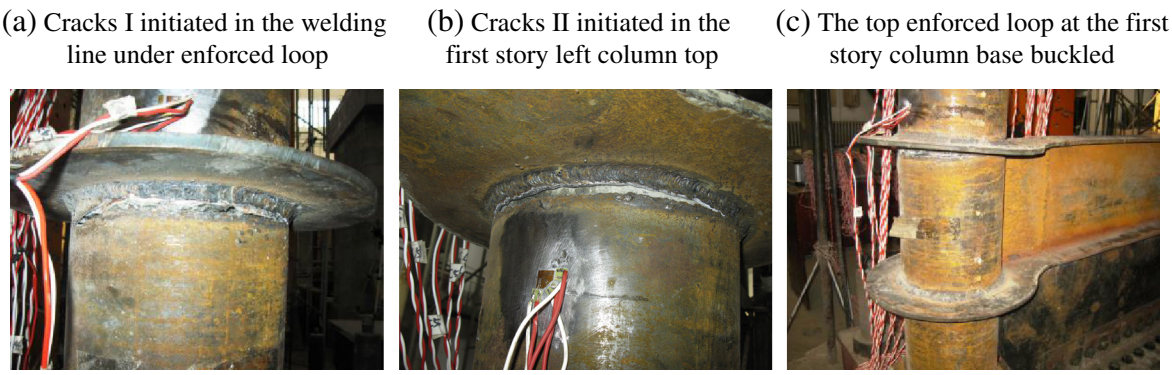

Fig. 23. Experimental phenomena of CF specimen. (a) Crack I initiated in the welding line under enforced loop. (b) Crack II initiated in the first story left column top. (c) The top enforced loop at the first story column base buckled.

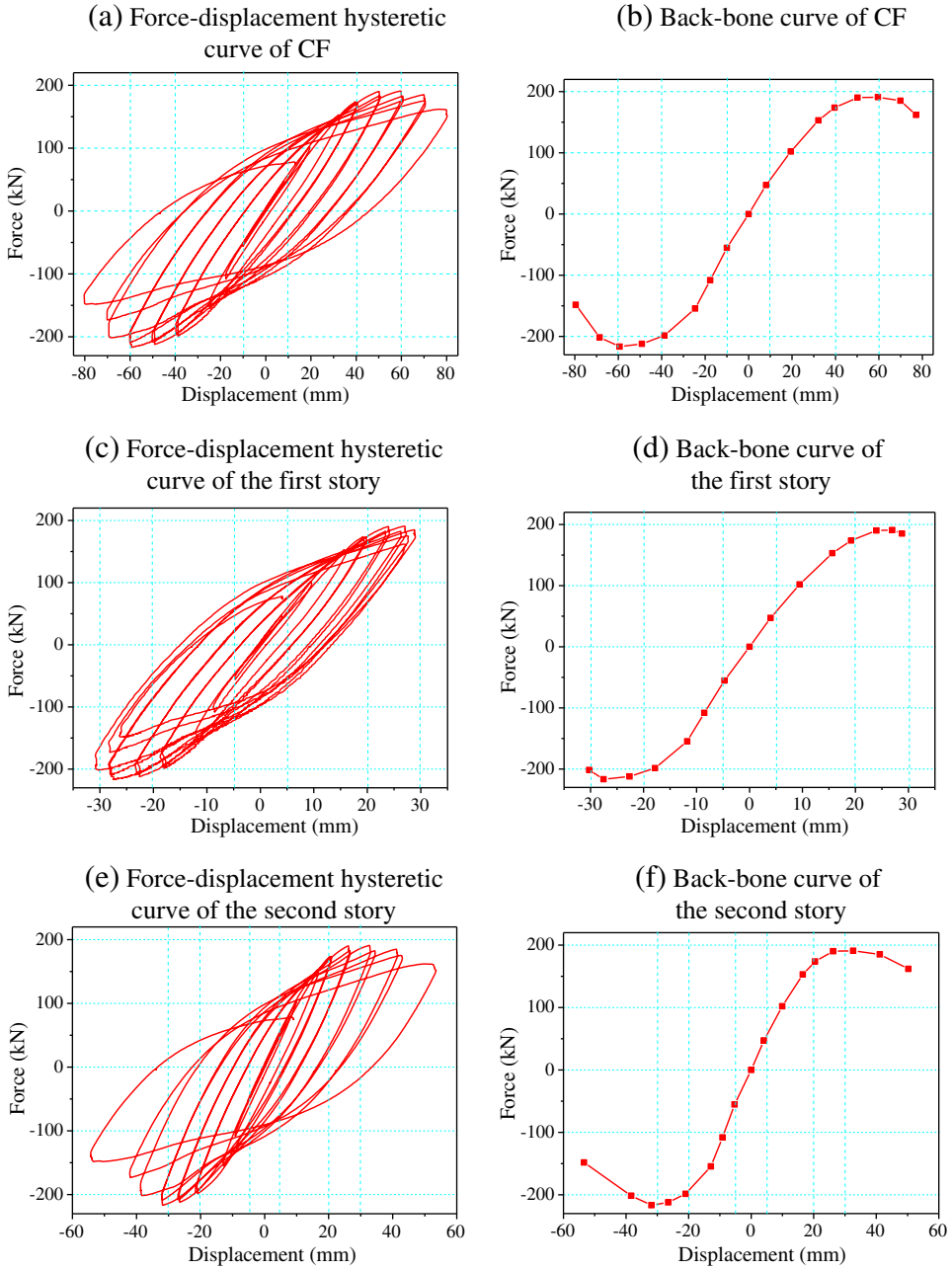

Fig. 24. Force-displacement hysteretic curves and back-bone curves of CF. (a) Force-displacement hysteretic curve of CF. (b) Back-bone curve of CF. (c) Force-displacement hysteretic curve of the first story. (d) Back-bone curve of the first story. (e) Force-displacement hysteretic curve of the second story. (f) Back-bone curve of the second story.

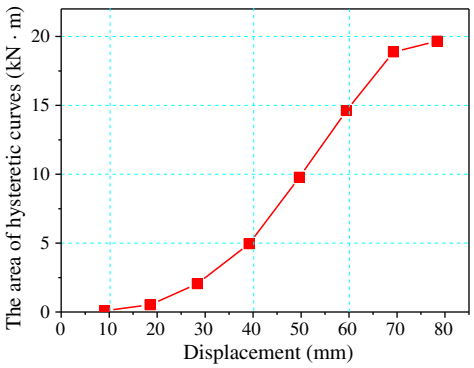

Fig. 25. The relationship curve of the area of hysteretic curves versus structural drift.

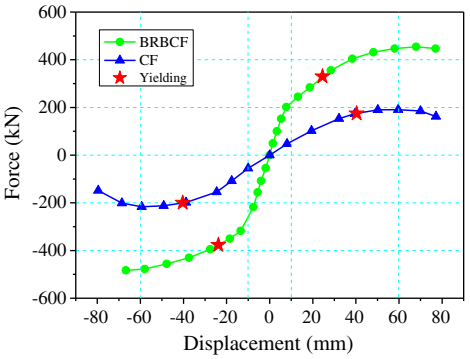

Fig. 27. Comparison of backbone curves.

force is 483 kN. In correspondence of maximum drift ratio, the negative stiffness approaches to zero and the positive stiffness is less than zero. As ductility is defined as the ratio of maximum drift and yielding displacement of the structure, i.e. Δ_{max}/Δ_y, so positive ductility is 2.77 and negative ductility is 2.81.

Fig. 17 shows the relationship curve of the area of hysteretic curves versus story drift, which indicates the energy dissipation of the specimen. The energy dissipation coefficient E was calculated according to Chinese code for seismic design of buildings (GB50011-2010), which is equal to the sum of area S_{ABC} and S_{CDA} divided by the sum of area S_{OBE} and S_{ODF}, as shown in Fig. 18. The relationship curve of the energy dissipation coefficient versus story drift is presented in Fig. 19, which represents the energy dissipation capacity of the specimen. The dissipation energy and the energy dissipation coefficient increase steadily after the frame members begin to yield, the maximum value of the energy dissipation coefficient reaches 0.904, which indicates that the hysteretic behavior and energy dissipation capacity of BRBCF are excellent.

Again using the strain gauge data to separate the response of various components, the hysteretic relationship of axial force versus axial deformation of BRB at top story before strain gauge failed is shown in Fig. 20. All BRBs have significant inelastic deformation and have stable hysteretic behavior and energy dissipation capacity.

6. Experimental results of CF

CF specimen and its dimensions are shown in Fig. 21. All the structural members of CF are same as those in BRBCF, which are made from the same materials and member sizes as the BRBCF frame.

As shown in Fig. 22, the yielding locations of components are indicated as circle points, the numbers show the sequence of structural members yielding.

At the top story drift ratio of 1/75 (drift of 20 mm), 1, 2, 3 points at the first story column base yielded. At the top story drift ratio of 40 mm, 4 point at the column base yielded; 5, 6 points at the column top connected to the actuator began yielding. All the yielding points are close to beam–column connections, meanwhile the stiffness of CF began to decrease. During the cycles of sequence between 30 mm and 40 mm, 7–10 points at the bottom and top flanges of middle beam at both ends yielded. At the top story drift ratio of 1/75, 11–13 points at the base and top of the first story column yielded. 1, 3 points at the steel tube buckled at the top story drift ratio of 1/75. The welding line of steel tube under enforced loop at the first story right column base fractured (Crack I), a crack (Crack II) initiated in the first story left column top and then developed to 2 mm width and 5–6 cm length. At the top story drift ratio of 1/30 (drift of 50 mm), 14, 15 points at the second story near the column base yielded. At frame drift of 60 mm, 16, 17 points at the first and second story right column top yielded. At the load level, Crack I developed to 3–4 mm width and 20 cm length and Crack II developed to 2–3 mm width and 12 cm length, the buckle of steel tube at 1 point developed. During the cycles of sequence at approximate top roof drift of 70 mm, 18 point at the web of middle beam adjacent to right beam–column connection yielded. Crack I developed to 4–5 mm width and half of steel tube circumference length (As shown in Fig. 23(a)) and Crack II developed to 4–5 mm width and 20 cm length (As shown in Fig. 23(b)). At top roof drift of 80 mm, 19–22 points at the first story column top yielded. Beam–column connections fractured at four inner angles of the first story, the cracks of welding lines of enforced loops at the first story right column top and left column base are about 1 cm width and more than half circumference length of steel tube. The top enforced loop at the first story column base buckled as shown in Fig. 23(c). According to the damage, the load-bearing capacity decrease to 85% ultimate load, the experiment was finished.

The base shear force versus roof drift and the story shear versus story drift relationships are shown in Fig. 24, the corresponding backbone

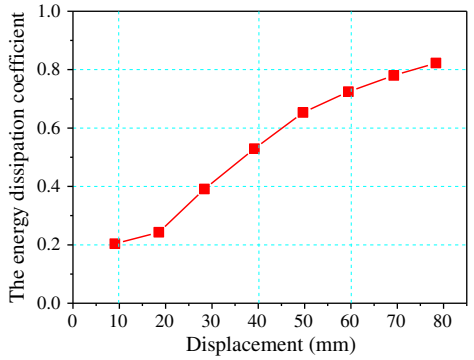

Fig. 26. The relationship curve of the energy dissipation coefficient versus structural drift.

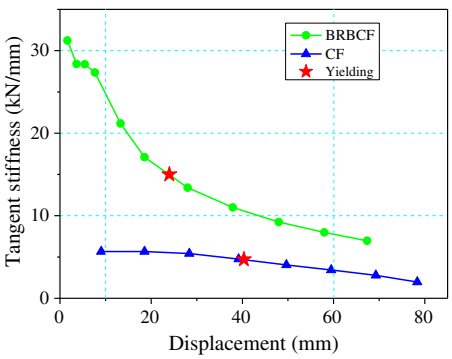

Fig. 28. Comparison of secant stiffness.

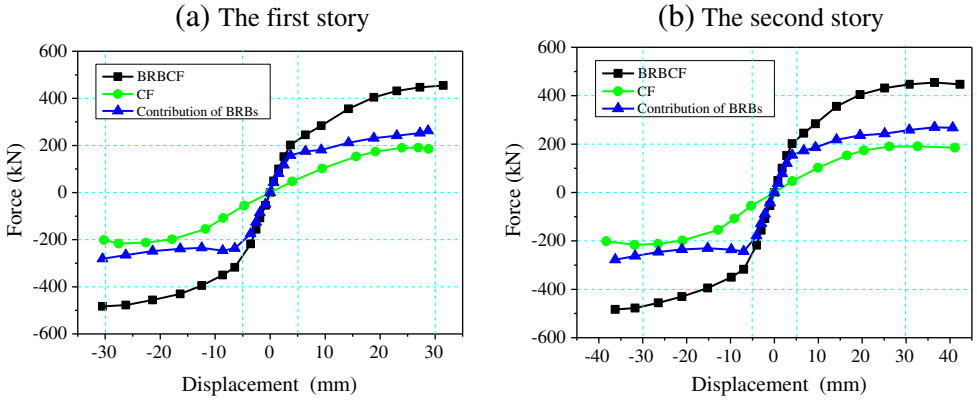

Fig. 29. The contribution of BRBs to structural load-bearing capacity. (a) The first story. (b) The second story.

Table 3
Comparison of load-bearing capacity of BRBCF and CF.

Specimens	Load direction	Yielding load and displacement		Maximum load and displacement		Ultimate displacement and corresponding load		V_{max}/V_y
		V_y (kN)	Δ_y (mm)	V_{max} (kN)	Δ_{max} (mm)	V_u (kN)	Δ_u (mm)	
BRBCF	Positive	312.74	24.51	454.27	67.97	446.66	77.00	1.45
	Negative	−376.28	−23.79	−482.96	−66.74	−482.96	−66.74	1.28
CF	Positive	175.02	40.37	190.97	59.58	161.87	77.13	1.09
	Negative	−200.46	−40.35	−216.67	−59.38	−148.07	−79.59	1.08

curves are also in Fig. 24. The figures show almost symmetrical mechanical behavior of CF, hysteretic curves are spindly and energy dissipation capacity isn't very good. During the larger displacements, the hysteretic curves don't coincide very well under the same displacement amplitude, the frame exhibits the deterioration of strength and stiffness when loaded cyclically.

Fig. 25 shows the relationship of the area of hysteretic curves versus structural drift, the energy dissipation coefficient versus structural drift relationship is presented in Fig. 26. The maximum value of the energy dissipation coefficient reaches 0.823.

7. Comparison of experimental results

Comparison of backbone curves and tangent stiffness of BRBCF and CF is shown in Figs. 27 and 28, the maximum displacements of two structures are within maximum roof drift of 80 mm.

Although the damage had occurred on the main frame, the curves show the stiffness of BRBCF didn't decrease sharply because BRBs didn't fail. The load-bearing capacity of CF decreased to below 85% maximum load at the ultimate displacement (top roof drift ratio of 1/39).

As shown in Fig. 29, the portions of the story shear force resisted by the frame and BRBs are separated, the BRBs resist most of the story shear force for the duration of the testing, especially before the yielding of BRBs. The contribution of BRBs is more than CF to structural stiffness and load-bearing capacity during the testing. The load-bearing capacity contribution of BRBs is 3.27 times and 4.59 times of CF at the positive and negative yielding displacement, and that is 1.36 times and 1.22 times at the positive and negative 1/50 frame drift ratio, which is structural elasto-plastic drift limit according to Chinese code for seismic design of buildings (GB50011-2010).

The yielding load and displacement, maximum load and displacement, ultimate displacement and corresponding load of BRBCF and CF are listed in Table 3. The ratios of maximum load and yielding load of BRBCF are 1.45 at positive displacement and larger than 1.28 at negative displacement; the ratios of maximum load and yielding load of CF are 1.09 at positive displacement and 1.08 at negative displacement. The tangent stiffness in elastic stage and plastic stage of BRBCF are 4.5 times and 2.5 times of CF respectively, the secant stiffness in elastic phase of BRBCF is 4.59 times of CF.

As shown in Table 4, the ratios of yielding load of BRBCF and CF are 1.79 at positive displacement and 1.88 at negative displacement; the ratios of ultimate load of BRBCF and CF are 2.38 at positive displacement and 2.23 at negative displacement; the ratios of maximum load and yielding load of BRBCF and CF are 1.33 at positive displacement and 1.19 at negative displacement. Compared to CF, the load-bearing capacity is improved distinctly after the frame installed with BRBs.

The hysteretic loops of BRBCF and CF at the displacement of 50 mm are shown in Fig. 30(a), Fig. 30(b) shows the relationship curve of the area of hysteretic curves versus structural drift, the energy dissipation coefficient versus structural drift relationship curve is presented in Fig. 30(c). As shown in Table 5, the area of total hysteretic loops of BRBCF is 3.44 times of CF, so the portion of energy dissipation of BRBs is 46.03 kNm, which is 2.44 times of CF. As shown in Fig. 30(c), the energy dissipation coefficient of BRBCF is 2.83 times of CF at the frame drift of 20 mm, and is 1.15 times of CF at maximum drift. The enhancement of energy dissipation coefficient is the role of BRBs. The positive ductility and negative ductility of BRBCF are 1.87 times and 1.91 times of CF respectively. The seismic performance is improved distinctly after CF installed with BRBs.

8. Conclusions

This paper describes the experimental work related to the test of one 1/3 scale 2-story 1-bay buckling-restrained braced composite frame (BRBCF), a same bare composite frame (CF) was tested to compare

Table 4
The load-bearing capacity ratios of BRBCF and CF.

Ratio	Load direction	V_y	V_{max}	V_{max}/V_y
BRBCF/CF	Positive	1.79	2.38	1.33
	Negative	1.88	2.23	1.19

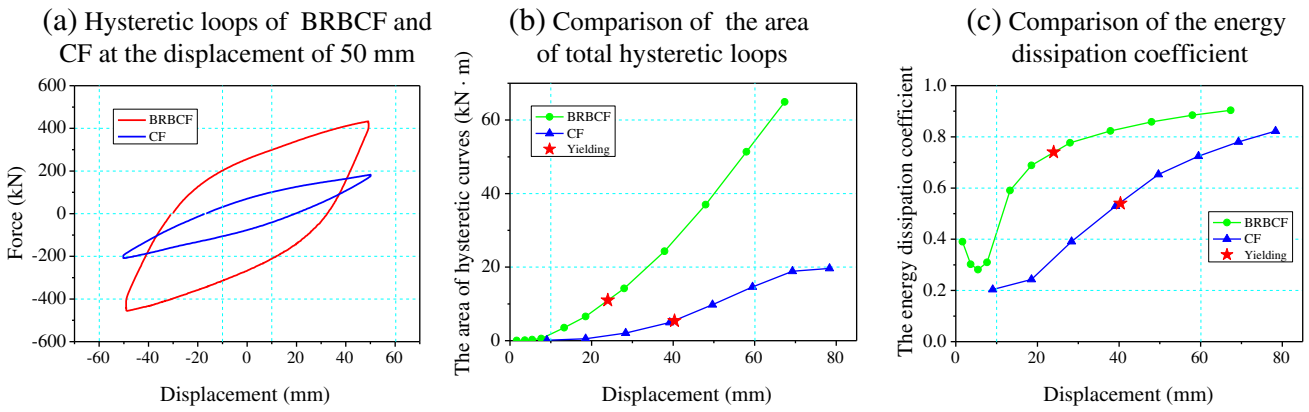

Fig. 30. Comparison of energy dissipation capacity (a) Hysteretic loops of BRBCF and CF at the displacement of 50 mm (b) Comparison of the area of total hysteretic loops (c) Comparison of the energy dissipation coefficient.

Table 5
Comparison of seismic performace of BRBCF and CF.

Specimens	The area of total hysteretic loops (kNm)		The energy dissipation coefficient		Positive ductility		Negative ductility	
	Value	Ratio	Value	Ratio	Value	Ratio	Value	Ratio
BRBCF	64.91	3.44	0.90	1.15	2.77	1.87	2.81	1.91
CF	18.88	1	0.78	1	1.48	1	1.47	1

with BRBCF. Based on the test and analysis, the following conclusions are given. BRBCF possesses good ductility and excellent energy dissipation capacity. BRBCF is excellent to demonstrate the mechanical behavior and seismic performance of the structural system. The structure can undergo many fully-reversed cycles without loss of stiffness and strength, and are also of great ductility, stable later stiffness and sustainable later load-bearing capacity. Compared to CF, it is shown that BRBs contribute significantly to the overall strength, stiffness, and energy dissipation capacity of the structural system and the structural system performed as intended. The yielding load and maximum load of BRBCF are 1.8 times and 2.2 times of CF respectively; the tangent stiffness in elastic stage and plastic stage of BRBCF are 4.5 times and 2.5 times of CF respectively; the positive ductility and negative ductility of BRBCF are 1.87 times and 1.91 times of CF respectively. The area of total hysteretic loops of BRBCF is 3.44 times of CF.

The welded splices beam–column–BRB connections are cheap joints and are convenient to install BRBs in construction site. The structure was designed according to Chinese codes, design base shear V_{des} = 140 kN, The yielding strength of BRBCF is 200 kN (= 1.43 V_{des}), which is larger than design base shear; the maximum load of BRBCF is about 3.2 times of design base shear. The ultimate roof displacement is about 70 mm, the maximum story drift ratio is large than 1/50. The experiment demonstrated BRBCF's ability to withstand major ductility demands. As the test indicated, the maximum frame drift prior to failure will be governed by the rotational capacity of the connection, not the axial deformation of the BRB. The test indicated that the flexural demands of the welded splices beam–column–brace connection should be considered in the design. Besides axial force, buckling-restrained braces in structures are also influenced by moment and shear. Larger rotational deformation capacity and moment resistance ability are needed to enable on the connection details of BRBCF. Compared to the BRB, the large force exerted by frame on the BRB gusset caused the gusset edges to fracture at high drift levels. So frame action should be considered in BRBCF design. The fracture and buckle of CHS steel tubes of composite columns at the first story bases are reasons for structural failure, the ratio of thickness and diameter of steel tube should be enlarged to resist the horizontal load.

Acknowledgments

The authors would like to acknowledge the support provided by National Science Foundation of China through projects (Grant Nos. 51008090, 51178150, 90715021), Open Research Fund of State Key Laboratory for Disaster Reduction in Civil Engineering (SLDRCE12-MB-04), Doctor Subject Foundation of the Ministry of Education of China (Grant No. 20102302120077), Natural Scientific Research Innovation Foundation in Harbin Institute of Technology (Grant No. HIT. NSRIF.2009),and Key Laboratory Foundation of Colleges and Universities of Beijing.

References

[1] Xie Q. State of the art of buckling-restrained braces in Asia. J Constr Steel Res 2005;61:727–48.
[2] Merritt S, Uang CM, Benzoni G. Subassemblage testing of corebrace buckling restrained braces. Technical report of department of structural engineering. San Diego, CA: University of California; 2003 [Report No.TR-2003/01].
[3] Black CJ, Makris N, Aiken ID. Component testing, stability analysis, and characterization of buckling restrained braced braces. Report No. PEER 2002/08. Berkeley, CA: Univ. of California; 2002.
[4] Black CJ, et al. Component testing, seismic evaluation and characterization of buckling-restrained braces. J Struct Eng ASCE 2004;130:880–94.
[5] Chou C-C, Chen S-Y. Subassemblage tests and finite element analyses of sandwiched buckling-restrained braces. Eng Struct 2010;32:2108–21.
[6] Wang C-L, Usami Tsutomu, Funayama Jyunki, Imase Fumiake. Low-cycle fatigue testing of extruded aluminium alloy buckling-restrained braces. Eng Struct 2013;46:294–301.
[7] Aiken ID, Mahin SA, Uriz P. Large-scale testing of buckling restrained braced frames. Proceeding of Japan Passive Control symposium. Yokohama, Japan: Tokyo Institute of Technology; 2002.
[8] Tsai KC, Hsiao BC, Lai JW, Chen CH, Lin ML, Weng YT. Pseudo dynamic experimental response of a full scale CFT/BRB composite frame. Proceeding of Joint NCREE/JRC Workshop on International Collaboration on Earthquake Disaster Mitigation Research, Tapei, Taiwan; 2003.
[9] Tsai KC, Loh CH, Hwang YC, Weng CS. Seismic retrofit of building structures with dampers in Taiwan. Proceeding of Symposium of Seismic Retrofit of Buildings and Bridges with Base Isolation and Dampers. Kyoto, Japan: Kyoto Univ; 2003.
[10] Christopulos AS. Improved seismic performance of BRBFs. [M.S. thesis] Seattle, WA: University of Washington; 2005.
[11] Roeder CW, Lehman DE, Christopulos A. Seismic performance of special concentrically braced frames with buckling restrained braces. Proceeding of 8th U.S. National Conf. on Earthquake Engineering. Oakland, CA: Earthquake Engineering Research Institute; 2006 [Paper No. 1503].

[12] Fahnestock LA, Ricles JM, Sause R. Experimental evaluation of a large-scale BRBF. J Struct Eng 2007;133:1205–14.
[13] Victoria RW, Fahnestock LA. Buckling-restrained braced frame connection performance. J Constr Steel Res 2010;66:65–74.
[14] Chou C-C, Chen P-J. Compressive behavior of central gusset plate connections for a buckling-restrained braced frame. J Constr Steel Res 2009;65:1138–48.
[15] Chou C-C, Liou G-S, Yu J-C. Compressive behavior of dual-gusset-plate connections for buckling-restrained braced frames. J Constr Steel Res 2012;76:54–67.
[16] Chou C-C, Liu J-H. Frame and brace action forces on steel corner gusset plate connections in buckling-restrained braced frames. Earthq Spectra 2012;28:531–51.
[17] Chou C-C, Liu J-H, Pham D-H. Steel buckling-restrained braced frames with single and dual corner gusset connections: seismic tests and analyses. Earthq Eng Struct Dyn 2012;41:1137–56.
[18] Jeffrey WB, Michel B. Cyclic testing of a buckling restrained braced frame with unconstrained gusset connections. J Struct Eng 2009;135:1499–510.
[19] Hikino Tsuyoshi, Okazaki Taichiro, Kajiwara Kouichi, Nakashima Masayoshi. Out-of-plane stability of buckling-restrained braces. Structures Congress © 2010 ASCE; 2010. p. 939–49.
[20] Chen C-H, Stephen Mahin. Seismic collapse performance of concentrically steel braced frames. Structures Congress © 2010 ASCE; 2010. p. 1266–74.
[21] Lin P-C, Tsai K-C, Wang K-J, et al. Seismic design and hybrid tests of a full-scale three-story buckling-restrained braced frame using welded end connections and thin profile. Earthq Eng Struct Dyn 2012;41:1001–20.
[22] Chen C-C, Chen S-Y, Liaw J-J. Application of low yield strength steel on controlled plastification ductile concentrically braced frames. Can J Civ Eng 2001;28:823–36.